

**REPORT DOCUMENTATION PAGE**

*Form Approved  
OMB No. 0704-0188*

The public reporting burden for this collection of information is estimated to average 1 hour per response, including the time for reviewing instructions, searching existing data sources, gathering and maintaining the data needed, and completing and reviewing the collection of information. Send comments regarding this burden estimate or any other aspect of this collection of information, including suggestions for reducing the burden, to Department of Defense, Washington Headquarters Services, Directorate for Information Operations and Reports (0704-0188), 1215 Jefferson Davis Highway, Suite 1204, Arlington, VA 22202-4302. Respondents should be aware that notwithstanding any other provision of law, no person shall be subject to any penalty for failing to comply with a collection of information if it does not display a currently valid OMB control number.  
**PLEASE DO NOT RETURN YOUR FORM TO THE ABOVE ADDRESS.**

1. REPORT DATE (DD-MM-YYYY) 06-05-2011		2. REPORT TYPE		3. DATES COVERED (From - To)	
4. TITLE AND SUBTITLE An Approach to Optimal Control of Electrodynamic Tethers in a Stochastically Varying Drag Environment				5a. CONTRACT NUMBER	
				5b. GRANT NUMBER	
				5c. PROGRAM ELEMENT NUMBER	
				5d. PROJECT NUMBER	
				5e. TASK NUMBER	
6. AUTHOR(S) Buck, Alexander James				5f. WORK UNIT NUMBER	
7. PERFORMING ORGANIZATION NAME(S) AND ADDRESS(ES)				8. PERFORMING ORGANIZATION REPORT NUMBER	
9. SPONSORING/MONITORING AGENCY NAME(S) AND ADDRESS(ES) U.S. Naval Academy Annapolis, MD 21402				10. SPONSOR/MONITOR'S ACRONYM(S)	
				11. SPONSOR/MONITOR'S REPORT NUMBER(S) Trident Scholar Report no. 396 (2011)	
12. DISTRIBUTION/AVAILABILITY STATEMENT This document has been approved for public release; its distribution is UNLIMITED					
13. SUPPLEMENTARY NOTES					
14. ABSTRACT Electrodynamic tethers offer a real option of zero-propellant orbital maneuvers in space. Using a linear controller to regulate a non-linear optimal control solution we can achieve reliable performance in spite of modeling error and environmental perturbations.					
15. SUBJECT TERMS electrodynamic tether, optimal control, feedback control, model error					
16. SECURITY CLASSIFICATION OF:			17. LIMITATION OF ABSTRACT	18. NUMBER OF PAGES 38	19a. NAME OF RESPONSIBLE PERSON
a. REPORT	b. ABSTRACT	c. THIS PAGE			19b. TELEPHONE NUMBER (Include area code)

U.S.N.A. – Trident Scholar project report; no. 396 (2011)

**An Approach to Optimal Control of Electrodynamic Tethers in a Stochastically Varying Drag Environment**

by

Midshipman 1/c Alexander J. Buck  
United States Naval Academy  
Annapolis, Maryland

---

(signature)

Certification of Advisor Approval

Commander Robert. E. Stevens, USN  
Aerospace Engineering Department

---

(signature)

---

(date)

Acceptance for the Trident Scholar Committee

Professor Carl E. Wick  
Associate Director of Midshipman Research

---

(signature)

---

(date)

USNA-1531-2

## Abstract

Electrodynamic Tethers (EDT's) offer a real option for zero-propellant orbital maneuvers in the near future. By controlling the electrical current through a long conductive cable aligned with the local vertical and in the presence of a magnetic field, the tether experiences an electrodynamic thrust. The local ionosphere provides the necessary electrons for the generation of an electrical current. Previous investigation has been focused on feed-forward or open-loop control schemes. Open-loop control methods are very susceptible to model error. The relevant models for an EDT system are the atmospheric density model and the magnetic field model. This paper will be concerned with errors in the atmospheric density model. The problem consists of two parts: solving the open loop non-linear optimal control problem and solving the associated linear feedback system to generate a control law.

To solve the first part we assume the orbit remains nearly circular. We apply the method of averaging to the state dynamics to track secular changes only. The short period motion of the spacecraft drives the shape of the control. We vary the coefficients on a five term modified Fourier series describing the tether's alternating electrical control current. The series is modified by using square waves rather than sine and cosine waves. The open-loop control solution is then used as reference in the feedback problem.

Solving the associated linear feedback system involves linearizing the state dynamics. Standard linearization yields a classic state-space structured system using state error to generate control corrections. We assume complete state feedback to simplify the solution. Treating the system as linear time invariant, we update the gain matrix once per orbit.

Results indicate this strategy improves performance and reliability of a system with model errors and un-modeled disturbances, particularly for maneuvers that remain in the LEO regime for an extended time.

Keywords: EDT, Electrodynamic Tether, Optimal Control, Feedback Control, model error

## **Acknowledgments**

I would like to acknowledge the Naval Academy and Trident Committee for giving me this amazing opportunity. I would also like to acknowledge Prof. Richard I. O'Brian for all his help with the linear control aspect of this project. Finally I would also like to acknowledge my advisor, CDR Stevens, for all his invaluable help in just about everything relating to this project.

## Table of Contents

Introduction	4
Derivation of Equations of Motion	10
Method of Averaging	16
Numerically Solve Nonlinear Optimal Control Problem	20
Linear Control Loop	21
Results & Analysis	23
Conclusion	27
Bibliography	29
Glossary	30
Appendix A	31
Appendix B	35
Appendix C	37

# An Approach to Optimal Control of Electrodynamic Tethers in a Stochastically Varying Drag Environment

Alexander J. Buck\*

## I. Introduction

The Low Earth Orbit (LEO) environment provides many scenarios where maneuvering in orbit—perhaps for an extended duration—is very necessary. The tenuous atmosphere is constantly slowing down spacecraft through drag, lowering their altitude; orbital debris can travel at relative speeds in excess of 10 km/s, fast enough to damage or destroy a spacecraft; and spacecraft are constantly being perturbed out of their orbit by small but constant effects such as solar wind, radiation pressure, slight variations in the gravitational field, and the gravitational influence from the Sun or Moon. For example, the International Space Station loses about 90 meters of altitude per day due to drag [1]. At that rate Station would lose over 30 km in one year which is 10% of its orbit altitude. To prevent the station from re-entering the atmosphere and burning up after just a few years, every few months resupply modules are launched with extra fuel to boost the station back up to a higher altitude. Orbital debris removal is another mission requiring large amounts of orbital maneuvering for extended periods of time. In early 2009 the Cosmos 2251—a defunct Russian communication satellite—collided with and destroyed Iridium 33—an operational US communications satellite. This event added roughly 1300 new pieces of debris larger than roughly 5cm radius—the approximate detectable radius of the US Space Surveillance Network sensors [2]. About once per year the ISS has to perform small maneuvers to avoid this debris, as it did in October, 2010 when a piece from a decommissioned NASA satellite broke off and had a close approach with the station. A 0.4 m/s boost maneuver was

---

\* Midshipman, Aerospace Engineering Department, m110966@usna.edu

executed to move the station away from the debris [3]. Instead of avoiding space debris, there are proposed missions to actively rendezvous with space debris in order to clean up the LEO environment. This mission profile has a very high maneuverability requirement in order to rendezvous with and capture debris in all its various orbits. These three reasons only begin to illustrate why we need to have maneuvering capabilities in orbit.

Chemical propulsion systems are currently the workhorse for this capability. These systems are largely reliable but there are certain problems with the technology. Chemical rockets rely on a reaction mass to produce the momentum exchange and pressure difference that generate thrust but are limited by the amount of propellant they can carry. Due to the disturbances previously mentioned, a satellite with no maneuverability becomes a large piece of orbital debris, or a “zombiesat” as was clearly shown in April, 2010 when Galaxy 15 turned unresponsive and began drifting towards its neighboring satellites [4]. Therefore before a satellite loses the ability to maneuver it is disposed of by re-entry or placement into a graveyard orbit. The more a spacecraft has to maneuver the faster it uses its available propellant, the shorter its lifespan is.

This can be problematic because satellites can be large and expensive and we want them to be operational for a very long time, often 15 years or more. To support a long mission life, a significant amount of propellant (mass) must be launched with the satellite. This extra mass must be launched and stored in the spacecraft. Considering that it costs roughly \$20,000 [5] to put one kilogram of mass into orbit, each kilogram of propellant can add significantly to launch costs.

Chemical rockets have been around for a long time and their fuel efficiencies—measured by specific impulse ( $I_{sp}$ )—have gotten better over time, but physical limitations of the combustion chemistry have more or less limited the best chemical motors to a vacuum specific impulse of

455 seconds. The specific impulse of a motor is directly linked to how much velocity change it can induce via the ideal rocket equation,

$$\Delta V = I_{sp} g \ln(m_i/m_f)$$

The subscripts  $i$  and  $f$  denoting initial and final masses, the difference being the propellant mass. For a mission that requires a total orbital velocity change ( $\Delta V$ ) of 10 km/s with a vacuum  $I_{sp}=455$  seconds, 90% of the initial launch mass must be fuel. This means a 100 kg spacecraft requires 900 kg of fuel to be launched along with it [6]. Using the \$20,000/kg mark cited earlier, the total launch cost for this system is roughly \$20 million.

There are other technologies being developed and used to help address some of the complications and drawbacks of chemical propulsion systems. One such technology is electric propulsion, which accelerates heavy ions through an electromagnetic field to produce thrust. Electric propulsion still depends on a reaction mass to generate thrust. This means there is still a finite fuel life, albeit considerably longer given the orders of magnitude higher  $I_{sp}$  values for these systems—on the order of 5,000-10,000+ seconds. For the same 10 km/s  $\Delta V$  mission requirement an electric propulsion motor operating at 5,000 seconds  $I_{sp}$  can achieve that with only 20% of the initial payload launch mass as propellant. To operate a 100 kg spacecraft would require 25kg of propellant to be launched along with it reducing the total launch mass by a factor of 8. As good as electric propulsion is there is another propulsion technology being tested called electrodynamic tethers (EDTs).



**Figure 2** – An Electrodynamic Tether (EDT). Credit Naval Research Labs

field,  $\mathbf{L}$  is a vector along the length of the tether and  $I$  is the control current causing the force. In

Figure 1 the force is directed out of the page. This is very different from the momentum

exchange through particle acceleration that

both chemical and electric propulsion thruster

designs operate under. Similar to electric

propulsion thrusters, EDTs can only generate a

very small but continuous thrust. Due to the

geometry of an EDT—we will assume this to

consist of two small subsatellites at either end

of the long conductive tether—the system is

dynamically stable in a nadir pointing orientation due to gravity gradient effects. The nadir

pointing orientation allows thrust generation but the system is constrained to thrusting in the

direction of the cross product of the  $\mathbf{B}$  field and the tether orientation,  $\mathbf{L}$ . This thrust direction

constraint combined with the extremely low thrust magnitude pose a significant challenge in

Electrodynamic tethers offer the real prospect of *zero-propellant* maneuvering in the earth orbit environment. This is achieved by using a very long conductive tether (Figure 2)—hence the name electrodynamic tether—to interact with the geomagnetic field via moving electrons (current). The resultant force on the conductive tether as described by the Lorentz force, the force on a current carrying wire in a magnetic field, is a propulsive force. The

Lorentz force is defined as  $\mathbf{F} = I\mathbf{L} \times \mathbf{B}$  where  $\mathbf{B}$  is the local magnetic

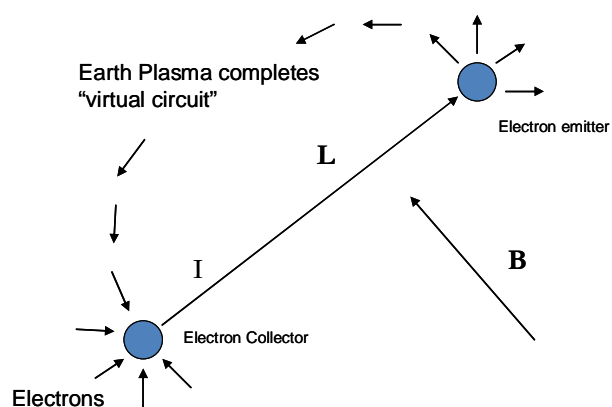


**Figure 1** – An EDT uses a conductive wire to interact with the geomagnetic field. Credit Naval Research Labs

controlling the spacecraft. Despite the system complexity, successful control of an EDT has been accomplished in simulations, with a wide range of orbital maneuvers being achievable.

While an inert tether is dynamically stable in its nadir pointing orientation, it will oscillate, or librate, both in and out of the orbital plane around its equilibrium point. The motion is similar to a swinging pendulum. These librations are due to the competing torques from gravity gradient, atmospheric drag, and if the tether is electrodynamic, the Lorentz force. Furthermore Palaez et al. [7] have demonstrated that a tether with a constant direct current will eventually become unstable. Controlling the Lorentz force by controlling the current has been shown to limit the amplitude of the libration to within acceptable limits, as shown by Lanoix et al. [8] and Hoyt [9]. Williams [10] demonstrated combined libration control and maneuvering control. He derived a numerical method for determining the optimal control of an EDT to maneuver between two desired orbits and also demonstrated that the natural librations can be exploited to achieve greater thrust by taking advantage of the changing tether orientation. This method works well for short duration maneuvers as he uses the instantaneous non-linear equations of motion, however; it requires significant computation time as a result. For longer scale maneuvers, on the order of weeks or months instead of hours, this method is both infeasible computationally and subject to significant accumulated round off error. As a consequence of the low thrust, the instantaneous state will only vary slightly from the average state, which slowly changes over many orbit revolutions. By applying the method of averaging to the equations of motion, Tragesser and San [11] were able to generate sub-optimal solutions to long duration maneuvers by using a periodic controller to change the average state of the system. Their work assumes a non-librating, nadir-pointing tether and no attempt was made to optimize the maneuvers. Stevens [12] took this method of averaging and combined it with optimal control theory to generate optimal control

solutions to a long duration tether orbital maneuver while considering libration. This approach utilizes a mathematical model of the system (i.e. dynamic equations of motion) and with optimization software numerically determines the minimum cost (i.e. time, or fuel consumption) trajectory to achieve the desired end state. The validity of this method is subject to the quality of the mathematical models it uses. A solution generated with no consideration of atmospheric drag in the model will not produce reliable performance in practice. Likewise, a solution generated with a poor model of atmospheric density will not produce reliable results when implemented in orbit. Our ability to accurately predict the atmospheric density in LEO is very poor. There are highly sophisticated statistical models that are very useful in satellite tracking and orbit determination but these models do not reliably predict the atmospheric density several weeks ahead of time. As such, the optimal control solution generated using these models will not reliably maneuver the spacecraft to the desired orbit. The purpose of this paper is to extend the work of Stevens by implementing feedback control to the optimal control maneuver in order to achieve reliable performance despite modeling inaccuracies.

This goal will be achieved in four steps as follows: (also visually represented in Figure 3):

- 1) Derive the equations of motion for a tether system from the Gaussian variation of parameters equations.
- 2) Numerically solve the non-linear optimal control problem (NLOCP) for the whole maneuver.
- 3) Linearize the averaged equations of motion and determine the linear quadratic regulator control law to accommodate a dynamic model with a time varying atmosphere.
- 4) Test the feedback controller within a numerical simulator to demonstrate reliable performance.

To produce a dynamic model we will assume:

- Near circular orbits ( $e \ll 1$ ).
- Negligible sensor error in feedback (complete state feedback).
- Perfect knowledge of true anomaly (true anomaly as the independent time variable).
- Constant nadir pointing tether orientation
- Periodic current control to match the periodic orbit environment
- Non-tilted dipole model of geomagnetic field

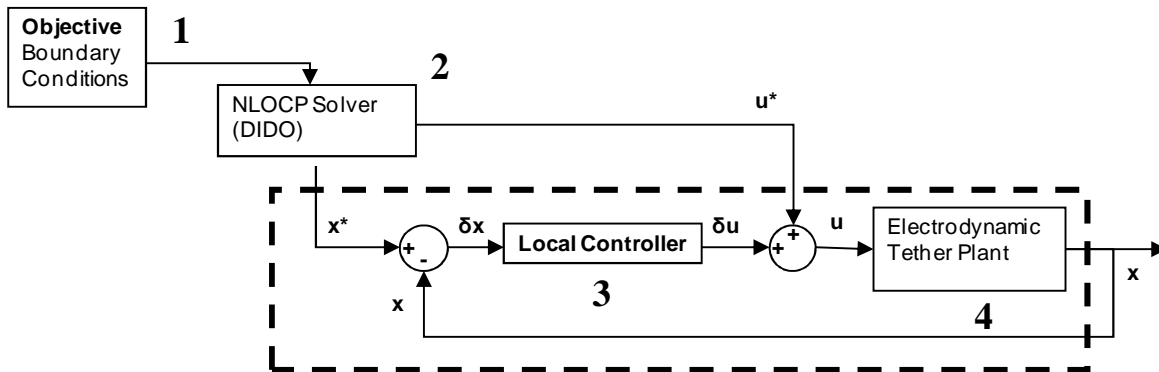
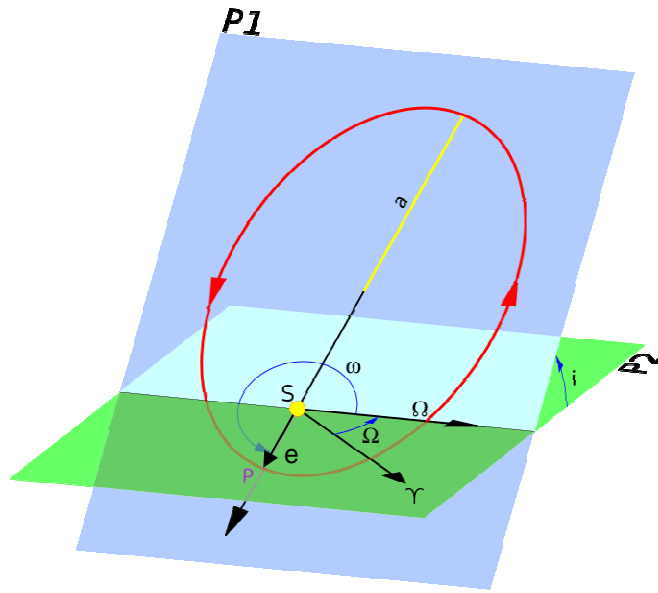


Figure 3 – Block diagram depiction of inner/outer loop structure

## II. Derivation of Equations of Motion

The main force driving the equations of motion is central body gravitation. We will also consider the influence of the next largest force in the low earth orbit environment which is atmospheric drag. To describe an orbit we require six pieces of information that comprise the *state vector* or *element set*. The orbit can be defined as a state vector in the form of position and velocity vectors or as an element set in the form of a scalar magnitude and angular positions. Position and velocity vector representations are not the most efficient method for describing orbits as the state values will constantly be changing due to periodic motion. Instead we choose an element set representation, in particular, the classical orbital elements (we in fact use a partial-

equinoctial element set, a distinction to be described later). In an unperturbed orbit that is only subject to gravitation influence, the classical orbital elements (COEs) do not vary with the exception of true anomaly. A visual representation of the six orbital elements is seen in Figure 4 [13].



**Figure 4 – The six classical orbital elements,  $a$ ,  $e$ ,  $i$ ,  $\Omega$ ,  $\omega$ ,  $v$ .** Credit: Brandir

These six states completely and uniquely define an orbit. The semi-major axis ( $a$ ) defines the size of the orbit, eccentricity ( $e$ ) defines the elongation of the orbit, inclination ( $i$ ) defines the orientation of the orbit with respect to the equator, argument of perigee ( $\omega$ ) defines where the lowest point of the orbit is with respect to the line of nodes, right ascension of the ascending node ( $\Omega$ ) defines the location of the ascending equatorial crossings (line of nodes) and true anomaly ( $v$ ) defines where the satellite is in the orbit with respect to perigee. They have been carefully chosen to be static in value during free motion. In forced or perturbed motion, Vallado [14] defines these variation-of-parameters (VOP) equations which describe their time rates of change due to any perturbing accelerations (the Gaussian form). Beginning with equation (1.1), a full derivation of the dynamics can be found in Appendix A

$$\begin{aligned}
\frac{da}{dt} &= \frac{2}{n\sqrt{1-e^2}} \left[ e \sin v f_R + \frac{p}{r} f_S \right] \\
\frac{de}{dt} &= \frac{\sqrt{1-e^2}}{na} \left[ \sin v f_R + \left( \cos v + \frac{e + \cos v}{1 + e \cos v} \right) f_S \right] \\
\frac{di}{dt} &= \frac{r \cos(v + \omega)}{na^2 \sqrt{1-e^2}} f_W \\
\frac{d\Omega}{dt} &= \frac{r \sin(v + \omega)}{na^2 \sqrt{1-e^2} \sin i} f_W \\
\frac{d\omega}{dt} &= \frac{\sqrt{1-e^2}}{nae} \left[ -\cos v f_R + \sin v \left( 1 + \frac{r}{p} \right) f_S \right] - \frac{r \cot i \sin(v + \omega)}{h} f_W \\
\frac{dv}{dt} &= \frac{na^2}{r^3} \sqrt{1-e^2} + \frac{\sqrt{1-e^2}}{nae} \cos v f_R - \frac{\sqrt{1-e^2}}{nae} \frac{2 + e \cos v}{1 + e \cos v} f_S
\end{aligned} \tag{1.1}$$

To avoid confusion with the semi-major axis ( $a$ ) or with forces ( $F$ ) we notate the perturbing accelerations as a lowercase  $f$ .

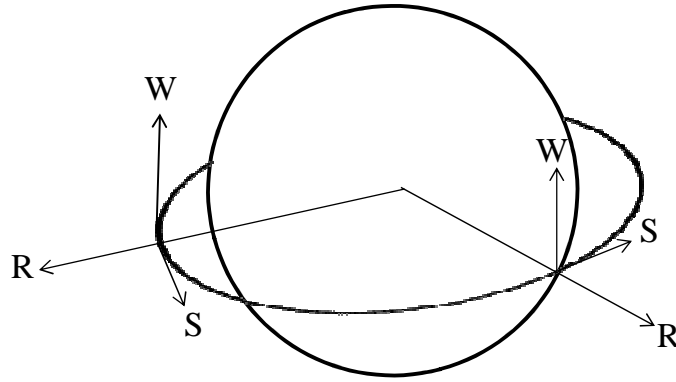


**Figure 5 – The RSW frame. Radial (R), In-track (S), Orbit normal (W).**

For the equation (1.1) the accelerations must be expressed in the Local Vertical Local Horizontal (LVLH) frame, sometimes also written as RSW. These axes are directed in the radial (R), in-track, (S), and orbit normal (W) directions.

### 1. Equinoctial Elements – $h$ and $k$

Our first step is to modify our element set. We do this because of singularities for zero eccentricity and the poor behavior of  $\omega$  and  $e$  for very small eccentricities. These considerations are very relevant because a working assumption is that the EDT orbit is at any time approximately circular ( $e \sim 0$ ). We replace the elements  $\omega$  and  $e$  with two elements borrowed from

the full equinoctial set described by Vallado [15]. We choose  $h$  and  $k$ , defined as,  $h = e \sin \nu$  and  $k = e \cos \nu$ . The classical pair, eccentricity and argument of perigee, define a vector (magnitude and direction respectively) that points towards perigee of the orbit, see Figure 6. For very small  $e$ , this vector can rapidly cross over the origin causing both  $e$  and  $\omega$  to rapidly change in an almost discontinuous manner (see Figure 7 and 8). For closer passes with the origin, the behavior would cause numerical errors, eventually becoming non-differentiable.

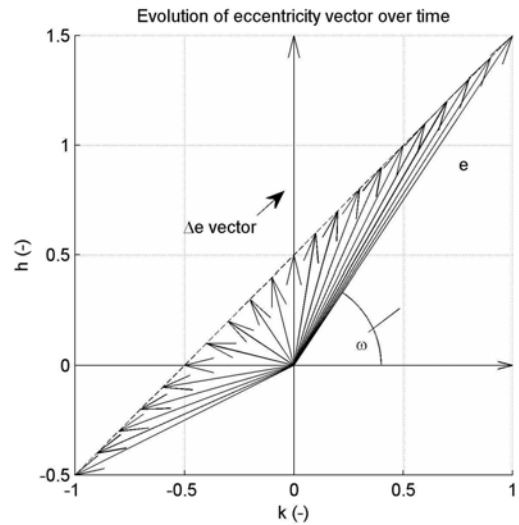


**Figure 6 - As the eccentricity vector crosses near or over the origin, the behavior becomes increasingly singular while equinoctial elements,  $h$  and  $k$  vary linearly.**

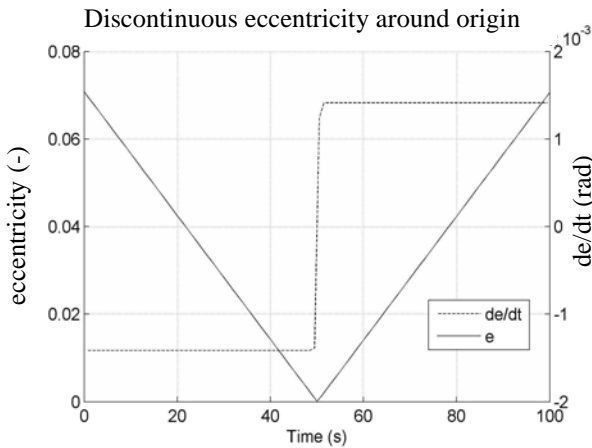


**Figure 7 – Discontinuous eccentricity around the origin**

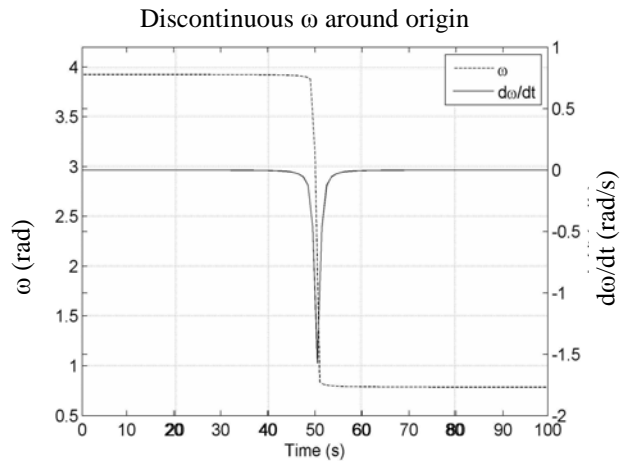


**Figure 8 – Discontinuous  $\omega$  around the origin**

The equinoctial elements by contrast represent the Cartesian components of this vector which avoid singularities when the orbit is circular. When the eccentricity vector passes by the origin, the equinoctial elements exhibit no discontinuities. By avoiding these singularities and rapidly changing values, the well behaved equinoctial elements  $h$  and  $k$  are much more suitable for accurate numerical analysis.

With this element substitution in mind we can now express the rates of change for the new elements. As a further reduction we apply our assumption of nearly circular orbits, whereby we ignore eccentricities  $\mathcal{O}(e^2)$  and smaller. In deriving the equations of motion we will eventually wish to find the averaged state dynamics which will require integration of the dynamic equations. To simplify the process of integration we eliminate time and allow true anomaly, the angular position, to be the independent variable. Changing the independent variable supposes the system has perfect knowledge of the true anomaly, which we take as a simplifying assumption. The resultant dynamics, equation (1.2), describe the changes in the element set due to any perturbing accelerations in the RSW frame.

$$\begin{aligned}
\frac{da}{dv} &= \frac{2a^3}{\mu_{\oplus}} \left[ e \sin \nu f_R + (1 - e \cos \nu) f_S \right] \\
\frac{di}{dv} &= \frac{a^2}{\mu_{\oplus}} (1 - 3e \cos \nu) \cos(\nu + \omega) f_W \\
\frac{d\Omega}{dv} &= \frac{a^2}{\mu_{\oplus}} (1 - 3e \cos \nu) \frac{\sin(\nu + \omega)}{\sin i} f_W \\
\frac{dh}{dv} &= \frac{a^2}{\mu_{\oplus}} \begin{bmatrix} -\cos(\nu + \omega) - h \sin 2\nu - 2k \cos^2 \nu \\ 2 \sin(\nu + \omega) + h \sin^2 \nu - 5k \sin \nu \cos \nu - 4h \cos^2 \nu \\ -k \sin(\nu + \omega) \cot i \end{bmatrix}^T \begin{bmatrix} f_R \\ f_S \\ f_W \end{bmatrix} \\
\frac{dk}{dv} &= \frac{a^2}{\mu_{\oplus}} \begin{bmatrix} \sin(\nu + \omega) - k \sin 2\nu - 2h \cos^2 \nu \\ 2 \cos(\nu + \omega) + k \sin^2 \nu + 5h \sin \nu \cos \nu - 4k \cos^2 \nu \\ h \sin(\nu + \omega) \cot i \end{bmatrix}^T \begin{bmatrix} f_R \\ f_S \\ f_W \end{bmatrix}
\end{aligned} \tag{1.2}$$

To continue we must now define the perturbing accelerations.

## 2. Perturbing Accelerations

There are two major sources of perturbing accelerations we will consider:

- Electrodynamic forces
- Atmospheric drag forces

We first will consider the electrodynamic forces on the tether. Using a non-tilted dipole model of the earth, equation (1.3), and our assumption that the tether remains nadir pointing we derive the electromagnetic perturbing accelerations on the tether (1.4) by the Lorentz force definition,  $\mathbf{F} = I\mathbf{L}\times\mathbf{B}$ .

$$\mathbf{B} = \frac{\gamma_m \mu_0}{r^3} \begin{bmatrix} -2 \sin(\nu + \omega) \sin i \\ \cos(\nu + \omega) \sin i \\ \cos i \end{bmatrix} \quad (1.3)$$

With the non-tilted dipole we express the perturbing accelerations as:

$$\begin{bmatrix} f_R \\ f_S \\ f_W \end{bmatrix}_{tether} = \frac{IL\gamma_m\mu_0}{ma^3} (1 + 3e \cos \nu) \begin{bmatrix} 0 \\ -\cos i \\ \cos(\nu + \omega) \sin i \end{bmatrix} \quad (1.4)$$

The acceleration is a function of the state vector,  $\mathbf{x} = [a \ i \ \Omega \ h \ k]^T$ , true anomaly ( $\nu$ ), and the current through the tether,  $I$  (the control). The remaining parameters are constants: tether length ( $L$ ), tether system mass ( $m$ ), magnetic constant ( $\mu_0 = 4\pi \cdot 10^{-7} \text{ N} \cdot \text{A}^{-2}$ ), and the dipole moment of the earth ( $\gamma_m = 4 \cdot 10^{22} \text{ A} \cdot \text{m}^2$ ).

Now we consider atmospheric drag forces. Using the standard definition of drag acceleration— $\mathbf{F}_{drag}/m = -\frac{1}{2} B^* \rho V^2 \hat{\mathbf{V}}$ , where  $B^* = \frac{C_D A}{m}$  is the inverse ballistic coefficient—and the flight path angle to define the velocity vector in terms of orbital elements, we can describe the atmospheric drag as a function of the orbital elements. Again, ignoring  $\mathcal{O}(e^2)$  and smaller terms we find the accelerations due to drag are:

$$\begin{bmatrix} f_R \\ f_S \\ f_W \end{bmatrix}_{Drag} = -\frac{1}{2} B^* \rho \frac{\mu}{a} \begin{bmatrix} e \sin \nu \\ 1 + 2e \cos \nu \\ 0 \end{bmatrix} \quad (1.5)$$

With these perturbing accelerations defined we write out fully the system dynamics as rates with respect to the fast time variable  $\nu$  and in terms of the control current  $I$ . We capture the

constant values in  $C_m = \frac{L\gamma_m\mu_0}{m\mu_\oplus}$ .

$$\begin{aligned}
\frac{da}{d\nu} &= 2C_m \cos i (1 + 2e \cos \nu) \cdot I \\
\frac{di}{d\nu} &= \frac{-C_m}{a} \sin i \cos^2(\nu + \omega) \cdot I \\
\frac{d\Omega}{d\nu} &= \frac{-C_m}{a} \sin(\nu + \omega) \cos(\nu + \omega) \cdot I \\
\frac{dh}{d\nu} &= \frac{C_m}{a} \cos i \left[ \frac{3h}{2} + \frac{2h}{e} \cos \nu + \frac{2k}{e} \sin \nu + \left( \frac{h}{2} + \frac{hk^2}{e^2} \right) \cos 2\nu + \left( \frac{k}{2} + \frac{k(k^2 - h^2)}{2e^2} \right) \sin 2\nu \right] \cdot I \\
\frac{dk}{d\nu} &= \frac{C_m}{a} \cos i \left[ \frac{3k}{2} + \frac{2k}{e} \cos \nu - \frac{2h}{e} \sin \nu + \left( \frac{k}{2} - \frac{kh^2}{e^2} \right) \cos 2\nu - \left( \frac{h}{2} + \frac{h(k^2 - h^2)}{2e^2} \right) \sin 2\nu \right] \cdot I
\end{aligned} \tag{1.6}$$

We can also write the dynamics in a much more compact form, which we will use for the remainder of this paper where the state is denoted as  $\mathbf{x}$  and  $\mathbf{A}_1$  and  $\mathbf{B}_1$  are matrices defined in Appendix A.

$$\frac{d\mathbf{x}}{d\nu} = \mathbf{A}_1(\mathbf{x}, \nu) + \mathbf{B}_1(\mathbf{x}, \nu)I \tag{1.7}$$

## II. Method of Averaging

So far the state dynamics are expressed as rates with respect to a fast time variable, the true anomaly. We call this “fast” time because it describes variations that occur within a single orbit on a short time scale. Numerical modeling with a fast independent variable is problematic for very long duration maneuvers. To accurately model each orbit and have a high enough “resolution” to the orbit many data points need to be solved for within each orbit. Maneuvers consisting of thousands of orbits then require tens to hundreds of thousands of node points. Over such long time spans, numerical round-off errors compound and can become significant.

Additionally, the computation time for solving the optimal control problem with thousands of nodes is infeasibly large. Because the orbit perturbations are small, orbit variations are small over short time spans and only exhibit observable secular changes over long time spans. It would be computationally advantageous to not model the periodic variations at all, and focus solely on the secular changes in the state as in Figure 7.

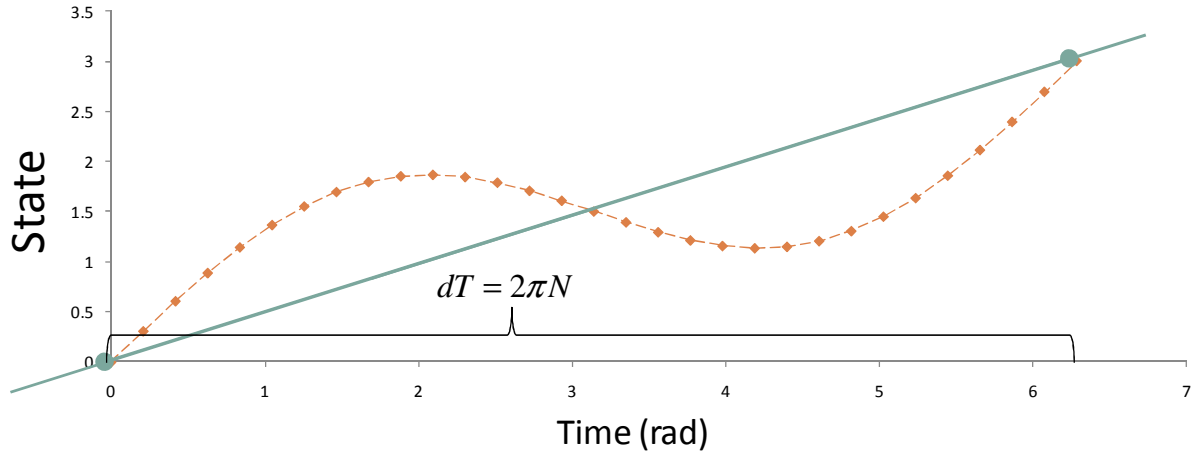


**Figure 7 – Averaging the dynamics over N integral orbits.**

This can be achieved through the method of averaging. The secular state changes occur slowly enough that we can consider them constant over some small, integral number of orbits, N. Averaging the dynamics over that time span has the effect of removing the periodic variations.

$$\frac{d\mathbf{x}}{dT} = \frac{1}{2\pi N} \int_0^{2\pi N} \frac{d\mathbf{x}}{dv} dv \quad (1.8)$$

The independent variable in the resulting equations is no longer a fast time variable ( $v$ ), but is now a slow time variable ( $T$ ). The slow Equation (1.8) now describes the secular changes in state values. These averaged states have no real meaning at any single instant in time, but serve to capture the changes in the system state over time.

To compute the integral in (1.8) requires knowledge of the variable current,  $I$ . Looking at equation (1.2) we see the accelerations,  $f$ , are multiplied by periodic functions that oscillate at the orbital frequency and twice the orbital frequency ( $\cos v$  or  $\sin v$  and  $\cos 2v$  or  $\sin 2v$ ). To get the

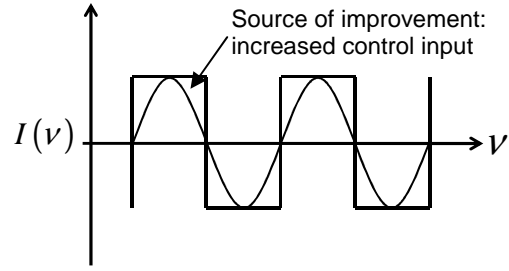


**Figure 8 – The square wave analog to a Fourier series.**

maximum change (i.e. never work against ourselves) we need to “push” in phase with the natural dynamics just like pushing a swing in sync with its motion. To do this we describe the current as a square wave analog to a Fourier series. The square wave aspect arises by using the sign of cosine and sine functions as opposed to the cosine and sine function themselves.

$$I = I_m \mathbf{u}^T \Psi = I_m \Psi^T \mathbf{u} \quad (1.9)$$

where  $\mathbf{u}$  and  $\Psi$  are,

$$\mathbf{u}^T = [u_1 \quad u_2 \quad u_3 \quad u_4 \quad u_5] \quad (1.10)$$

$$\Psi^T = \text{sign}([1 \quad \cos(v) \quad \sin(v) \quad \cos(2v) \quad \sin(2v)]) \quad (1.11)$$

and  $I_m$  is the maximum RMS current. The control coefficients,  $u_1$  through  $u_5$ , are bounded as:

$$\begin{aligned} -1 &\leq u_1 \leq 1 \\ i \in [2, 5], \quad -\sqrt{2} &\leq u_i \leq \sqrt{2} \end{aligned}$$

The difference between  $u_1$  and  $u_2$  through  $u_5$  is because the  $u_1$  term applies to the DC term while the  $u_2$  through  $u_5$  terms apply to the AC sinusoidal terms. This satisfies the RMS current constraint,

$$I_{RMS}^2 = u_1^2 + \frac{1}{2} \sum_{i=2}^5 u_i^2 \leq I_{RMS, Limit}^2 \quad (1.12)$$

Again note the sign function in equation(1.11), this is a departure from previous work in the field by Stevens [16]. In his work Stevens assumed a sinusoidal periodic controller. We have found a ~27% improvement, a factor of  $\left(\frac{4}{\pi}\right)$ , by using square wave periodic controller. Visually the improvement is seen as the increased area under the square wave and above the sine or cosine wave (Figure 8). As the cosine or sine function approaches zero the current would decrease in a sinusoidal controller while this square wave controller keeps the control input (current) high until the natural switching point of the dynamics at which point the natural tendency of the dynamics reverses and so the influence of the coefficient switches from positive to negative (as  $\sin v$  passes from positive to negative the effect of its  $u$  coefficient switches sign).

With the system dynamics fully described by (1.2), (1.4), and (1.5), we now undertake the method of averaging. The matrices found below are explicitly defined in Appendix B. By combining those three equations and rearranging we can express the state dynamics in a matrix form.

$$\frac{d\mathbf{x}}{d\nu} = \mathbf{A}_1(\mathbf{x}, \nu) + \mathbf{B}_1(\mathbf{x}, \nu)\Psi^T(\nu)\mathbf{u} \quad (1.13)$$

Vector  $\mathbf{A}_1$  represents the changes due to uncontrolled perturbations, i.e. drag. Vector  $\mathbf{B}_1$  represents the changes due to electrodynamic forces caused by some current  $I$  in the tether. It is possible to extract the fast time dependence from  $\mathbf{A}_1$  and  $\mathbf{B}_1$ , resulting in  $\mathbf{A}'(\mathbf{x})\Phi(\nu)$  and  $\mathbf{B}'(\mathbf{x})\Phi(\nu)$ . This simplifies the integration by only requiring integration of periodic functions of the fast time variable. Most of the terms in the product average out to zero. Only non-periodic secular terms survive the integration.

The resulting averaged dynamic equations of motion are as follows:

$$\frac{d\mathbf{x}}{dT} = \mathbf{A}_2(\mathbf{x}) + \mathbf{B}_2(\mathbf{x})\mathbf{u} \quad (1.14)$$

where

$$\mathbf{A}_2 = \frac{1}{2\pi N} \mathbf{A}'_1 \int_0^{2\pi N} \Phi(v) dv \quad \text{and} \quad \mathbf{B}_2 = \frac{1}{2\pi N} \mathbf{B}'_1 \int_0^{2\pi N} \Phi(v) \Psi^T(v) dv \cdot \mathbf{u}$$

Complete expressions for the preceding equations can be found in Appendix B. Equation (1.14) will serve as the basis for the remaining two steps.

### III. Numerically Solve Nonlinear Optimal Control Problem

The optimal control problem (OCP) is to find the control vector that will maneuver from a starting point to a final end point while minimizing some cost of the problem. Common OCP's are minimum fuel maneuvers; however as EDTs are not fuel limited we seek minimum time orbit transfers. To formally pose the OCP we must find the control function that will:

$$\text{Minimize the cost function,} \quad J = \phi(\mathbf{x}(t_f), t_f), \quad (2.1)$$

$$\text{subject to the dynamic constraints} \quad \dot{\mathbf{x}} = \mathbf{f}(\mathbf{x}, \mathbf{u}), \quad (2.2)$$

$$\text{boundary constraints,} \quad \boldsymbol{\varphi}(\mathbf{x}(t_f), t_f) = \mathbf{0}, \quad (2.3)$$

$$\text{and path constraints,} \quad \mathbf{g}(\mathbf{x}, \mathbf{u}) = \mathbf{0}. \quad (2.4)$$

$$\text{We then construct the Hamiltonian as} \quad H = \boldsymbol{\lambda}^T \mathbf{f} \quad (2.5)$$

$$\text{and the auxiliary function} \quad \Phi = \phi + \mathbf{v}^T \boldsymbol{\varphi} \quad (2.6)$$

where  $\boldsymbol{\lambda}$  is the costate vector and  $\mathbf{v}$  is a Lagrange multiplier. The necessary conditions for

$$\text{optimality are then the adjoint equations} \quad \dot{\boldsymbol{\lambda}} = -\frac{\partial H}{\partial \mathbf{x}} \quad (2.7)$$

$$\text{and the control optimality condition} \quad \frac{\partial H}{\partial \mathbf{u}} = \mathbf{0} \quad (2.8)$$

$$\text{subject to the transversality conditions} \quad \boldsymbol{\lambda}(t_f) = -\frac{\partial \Phi}{\partial \mathbf{x}} \Big|_{t=t_f} \quad (2.9)$$

and 
$$\left(\frac{\partial \Phi}{\partial t} + H\right) \Big|_{t=t_f} = 0 \quad (2.10)$$

From these necessary conditions we have a two point boundary value problem. Conceptually we have a set of coupled partial differential equations consisting of state dynamics (equation (2.2)) and costate dynamics (equation (2.7)) with various initial or final conditions. There are many methods for solving such systems numerically. We implement a program called DIDO to find a candidate optimal control function. The reason we chose this software is that it provides quick and accurate solutions without a first guess of the solution. Additionally the software is easy to use and it does not require the user to fully understand pseudospectral (PS) methods (the method used internally to find a solution). The user simply has to write the OCP much as they would on paper (or as above). The PS method does not use propagation and thus it is not susceptible to the round-off errors associated with other methods. For a full description of PS methods and their benefits see Refs [17], [18].

#### **IV. Linear Control Loop**

The optimal control solution is a pure open-loop control and assumes a perfect dynamic model of the system. In reality however, poor density and geomagnetic field models can lead to significant errors. To combat these inaccuracies and ensure reliable performance we introduce linear feedback as shown in Figure 3. Due to the exceptionally small thrust produced by an EDT, maneuvers happen over very long time scales. The states change slowly and can be considered to be constant within a single orbit period. With this assumption we linearize the dynamics from (1.14) with the intent of generating a linear-quadratic regulator (LQR) control law. The linearized dynamics we generate here will have state dependent gains. To maintain this as a linear time invariant system we update the gains once per orbit. The computation time for this

method is short compared to the hold time, with at most several seconds for the computation and 90 minutes of orbit at minimum. This avoids treating the system as linear time varying by doing a zero order hold—computing the gains at the beginning of the orbit with the states at that time and not updating until the next orbit.

Using the following procedure (fully developed in Appendix C) we linearized the averaged equations of motion.

$$\dot{\mathbf{x}} = \mathbf{f}(\mathbf{x}, \mathbf{u}) \quad (3.1)$$

Making a first order approximation of we say that

$$\mathbf{f}(\mathbf{x} + \delta\mathbf{x}, \mathbf{u} + \delta\mathbf{u}) = \mathbf{f}(\mathbf{x}, \mathbf{u}) + \mathbf{f}_x \delta\mathbf{x} + \mathbf{f}_u \delta\mathbf{u} \quad (3.2)$$

We can reduce this to the following

$$\delta\dot{\mathbf{x}} = \mathbf{f}_x \delta\mathbf{x} + \mathbf{f}_u \delta\mathbf{u} \quad (3.3)$$

The subscripts on  $\mathbf{f}$  denote the Jacobian of  $\mathbf{f}$  with regards to the state or control vector, as appropriate. For the linear system, Equation (3.3), with the following quadratic cost function

$$J = \int_{t_0}^{t_f} (\mathbf{x}^T \mathbf{Q} \mathbf{x} + \mathbf{u}^T \mathbf{R} \mathbf{u}) dt \quad (3.4)$$

The feedback control law that minimizes the cost is

$$\delta\mathbf{u} = -\mathbf{K} \delta\mathbf{x} \quad (3.5)$$

where  $\mathbf{K}$  is the solution the linear quadratic regulator problem and is given by

$$\mathbf{K} = \mathbf{R}^{-1} \mathbf{B}^T \mathbf{P} \quad (3.6)$$

and  $\mathbf{P}$  is the solution to the continuous time Riccati differential equation.

As we are assuming no sensor feedback we are able to define a state space system with  $\mathbf{A} = \mathbf{f}_x$ ,  $\mathbf{B} = \mathbf{f}_u$ . Upon proper definition of weighting matrices,  $\mathbf{Q}$  and  $\mathbf{R}$  this is now sufficient information to solve for the LQR gain matrix,  $\mathbf{K}$ . We generate a solution using the built-in LQR(...) function in MATLAB 7.10.0 (R2010a).

The candidate solution output from DIDO consists of averaged states thus a simple interpolation of those would not give us an appropriate reference trajectory. The instantaneous trajectory is known to have periodic oscillations (the entire reason for averaging to begin with), and so to generate the reference trajectory we propagate forwards one orbit using the state predicted by DIDO as the initial state. This method of on-the-fly reference generation avoids the numerical issues that arise if the entire reference is propagated from the beginning. Numerical propagation over a significant number of time steps accumulates round-off errors. For maneuvers lasting 100 orbits and each orbit consisting of roughly 5-10,000 time steps there is considerable room for accumulated errors. The problem is only compounded as the maneuver duration is increased. In our method the propagating time span is at most one orbit period thus there is no significant accumulated round off error.

## **V. Results & Analysis**

To test the control law we must simulate the system numerically because we cannot recreate the EDT dynamics physically on the ground. Using MATLAB we created a simulator, the structure of this process is captured in Figure 9. This is essentially identical to the block diagram presented earlier (Figure 3), the main difference being the “Plant” is now simply another numerical propagator with modeling error introduced rather than a physical system.

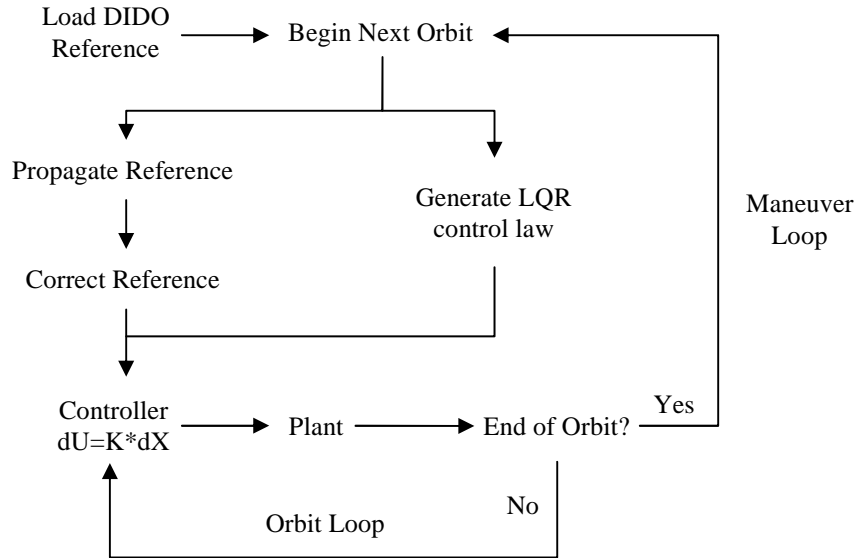


**Figure 9 – Flowchart of Control Law testing. Generate the control law and also generate the corrected reference. Iterate through the Orbit Loop until one full orbit has passed then restart the process for the next orbit.**

During numerical testing (using the above scheme) we sought to characterize the performance of a linear controller when atmospheric density model errors were introduced. To implement these errors we applied a lognormal distribution to the density. Measured data for altitudes ranging from 120km up to 750km have proven to be consistent with a lognormal distribution rather than the more common normal distribution, [19], [20]. The lognormal distribution is appropriately named because the log of the values is normally distributed. Lognormally distributed values,  $X$ , can be generated from a set of normally distributed numbers,  $Z$ , by

$$X = e^{Z\sigma + \mu} \quad (4.1)$$

where  $\sigma$  is the standard deviation of the logarithmic values,  $\ln(X)$ , and  $\mu$  is their mean. The mean is obtained in a table look-up of the 1976 Standard Atmosphere and the standard deviation is fixed at 1% of the mean. For this example a mean of  $10^{-11} \text{kg m}^{-3}$  was chosen purely for illustrative purposes.

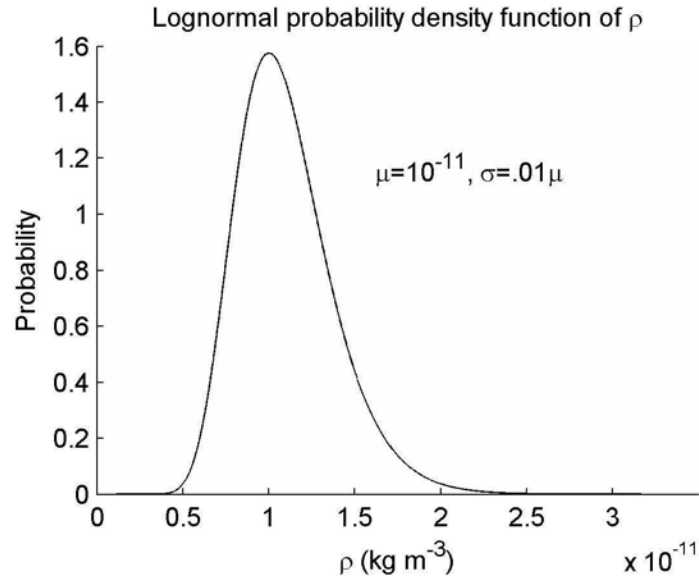


**Figure 10 – The probability density function for density is a log-normal distribution.**

Considering the linear system, the “noise” due to density variations is not white however; the values do have a mean of zero because the lognormal values only ever occur with a -1 attached to it, shifting them over 0. Comparing this shifted lognormal distribution with a Gaussian distribution for low values of standard deviation ( $<0.1$ ) we find that the two distributions are markedly similar, with only a slight skew to the right in the lognormal distribution. Under this premise, linear quadratic control is still valid, though not “optimal” because of the non-white noise. Using this method we set about to demonstrate the performance under the following conditions.

Maximum altitude raise in a fixed time span:

Initial Altitude : 250km

Initial Inclination : 1 degree

Initial Eccentricity : .051

Duration : 20 orbits

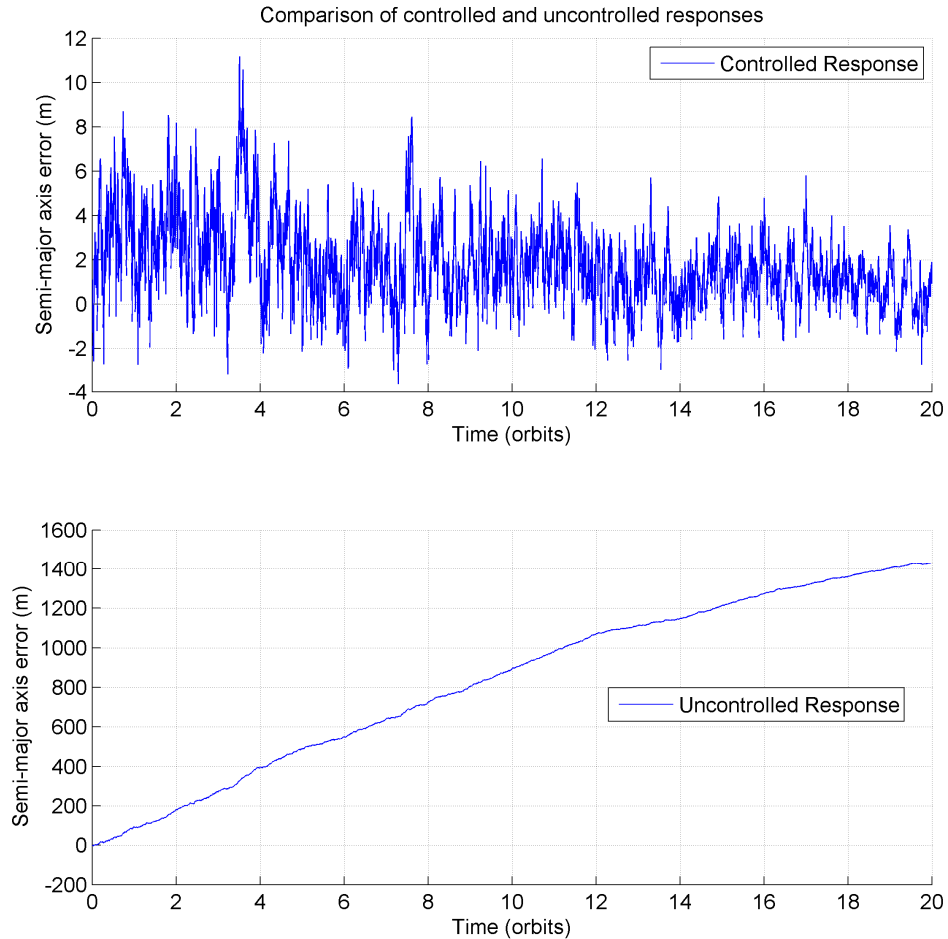


**Figure 11 – A comparison of controlled and uncontrolled responses during an orbit raise maneuver.**

The “controlled” scenario is the scenario where we apply linear feedback control to maintain the reference state. The “uncontrolled” scenario is the scenario where we apply no feedback and only have the reference optimal control as input. The controlled system remains bounded around zero error while the uncontrolled system has a state error that grows unbounded. After 20 orbits, which is roughly one and a half days, the state error is already approaching 1.5 km.

It is interesting to note the bias in the error towards positive altitude errors. We can explain this by again looking at the density distribution. The lognormal distribution has a slight skew to the right, meaning slightly higher densities more often. Higher densities would create a larger drag force, which would tend to reduce the orbit altitude. The error is computed as the difference

between the reference and the measured state, so for altitudes that are decreasing faster than expected, the state error tends towards the positive. This causes a steadily increasing state error in the uncontrolled response (the error is “noisy” but it is overlaid onto a roughly linearly increasing component). In the controlled scenario we see a steady state bias towards the positive. The bias is again due to the non-white (lognormal) distribution of the atmospheric density noise. The LQR method only generates the optimal gain matrix for white noise systems so the emergence of a steady state error is due applying LQR to lognormal noise.

## VI. Conclusion

We have successfully applied linear feedback control principles to a non-linear optimal control problem, specifically electrodynamic tether maneuvers. We have demonstrated a flaw with existing non-linear optimal control methodologies due to model uncertainties. Under solely the influence of the “optimal control” when the atmospheric density varies lognormally, there is introduced a significant state error. After applying linear feedback control via a linear quadratic regulator, the state errors remain bounded. This method allows for reliable and predictable, if perhaps slightly sub-optimal, performance of an electrodynamic tether.

There are also many ways to extend the work completed here. A more sophisticated geomagnetic field model or one with model uncertainties can be implemented. Other smaller perturbations can be considered such as solar radiation pressure and non-spherical earth dynamics. Additionally, linear feedback control methods other than linear quadratic regulators can be investigated for better performance and reduced steady state error when subject to lognormal noise. Such improvements will further enhance the reliability this method provides to precision maneuvering of electrodynamic tethers.

- 
- [1] "Space Math @ NASA" <http://spacemath.gsfc.nasa.gov/weekly/5Page35.pdf>
- [2] Kelso, T. S., "Analysis of the Iridium 33-Cosmos 2251 Collision," 2009 AMOS Technical Conference, September 2009,
- [3] "Orbital Debris Quarterly News" Volume 15 Issue 1, January 2011, NASA JSC
- [4] "Dealing with Galaxy 15: Zombiesats and on-orbit servicing" – Brian Weeden, *The Space Review*, 24 May, 2010, <http://goes.gsfc.nasa.gov/text/Zombiesats.pdf>
- [5] "Space Transportation Costs: Trends in Price Per Pound to Orbit 1990-2000", Futron Corporation, September 6, 2002.
- [6] Vallado, D., A., "Fundamentals of Astrodynamics and Applications", 3rd Ed., Microcosm Press, Hawthorne, CA, 2007.
- [7] Pelaez, J., Lorenzini, E. C., Lopez-Rebollal, O., and Ruiz, M., "A New Kind of Dynamic Instability in Electrodynamic Tethers," *Journal of the Astronautical Sciences*, Vol. 48, No. 4, 2000, pp. 449-476.
- [8] Lanoix, E. L. M., Misra, A. K., Modi, V. J., and Tyc, G., "Effect of Electromagnetic Forces on the Orbital Dynamics of Tethered Satellites," *AAS/AIAA Spaceflight Mechanics Meeting*, edited by C. A. Kluever, B. Neta, C. D. Hall, and J. M. Hanson, Univelt, San Diego, CA, 2000, pp. 1347-1365.
- [9] Hoyt, R. P., "Stabilization of Electrodynamic Space Tethers," *Proceedings of Space Technology and Applications International Forum (STAIF-2002)*, American Inst. of Physics, Melville, NY, 2002, pp. 570-577.
- [10] Williams, P., "Optimal Orbital Transfer with Electrodynamic Tether," *Journal of Guidance, Control, and Dynamics*, Vol. 28, No. 2, 2005, pp. 369-371.
- [11] Tragesser, S. G., and San, H., "Orbital Maneuvering with Electrodynamic Tethers," *Journal of Guidance, Control, and Dynamics*, Vol. 26, No. 5, 2003, pp. 805-810.
- [12] Stevens, R. S., "Optimal Control of Electrodynamic Tether Satellites" Air Force Institute of Technology, Wright-Patterson AFB, Ohio, June 2008
- [13] ArtMechanic, Wikimedia Commons, [http://en.wikibooks.org/wiki/File:Orbital\\_elements.svg](http://en.wikibooks.org/wiki/File:Orbital_elements.svg)
- [14] Vallado, D., A., "Fundamentals of Astrodynamics and Applications", 3rd Ed., Microcosm Press, Hawthorne, CA, 2007.
- [15] Ibid.
- [16] Stevens, R. S., "Optimal Control of Electrodynamic Tether Satellites" Air Force Institute of Technology, Wright-Patterson AFB, Ohio, June 2008
- [17] Gong, Q., Fahroo, F., Ross, I.M., "Spectral Algorithm for Pseudospectral Methods in Optimal Control," *Journal of Guidance, Control, and Dynamics*, Vol. 31, No. 3, 2008.
- [18] Trefethen, L. N., *Spectral Methods in Matlab*, SIAM, Philadelphia, PA, 2000
- [19] Prag, A. B., "A Comparison of the MSIS and Jacchia-70 Models with Measured Atmospheric Density Data in the 120 to 200 km Altitude Range," Aerospace Corp., El Segundo, CA, 1983
- [20] Bezděk, A., "Lognormal distribution of the observed and modeled neutral thermospheric densities," *Studia Geophysica et Geodaetica*, Vol. 51, No. 3, 2007, pp. 461-468.

## Bibliography

- ArtMechanic, Wikimedia Commons, [http://en.wikibooks.org/wiki/File:Orbital\\_elements.svg](http://en.wikibooks.org/wiki/File:Orbital_elements.svg)
- Bezděk, A., “Lognormal distribution of the observed and modeled neutral thermospheric densities,” *Studia Geophysica et Geodaetica*, Vol. 51, No. 3, 2007, pp. 461-468.
- Hoyt, R. P., “Stabilization of Electrodynamic Space Tethers,” *Proceedings of Space Technology and Applications International Forum (STAIF-2002)*, American Inst. of Physics, Melville, NY, 2002, pp. 570-577.
- Kelso, T. S., “Analysis of the Iridium 33-Cosmos 2251 Collision,” 2009 AMOS Technical Conference, September 2009,
- Lanoix, E. L. M., Misra, A. K., Modi, V. J., and Tyc, G., “Effect of Electromagnetic Forces on the Orbital Dynamics of Tethered Satellites,” *AAS/AIAA Spaceflight Mechanics Meeting*, edited by C. A. Kluever, B. Neta, C. D. Hall, and J. M. Hanson, Univelt, San Diego, CA, 2000, pp. 1347-1365.
- Pelaez, J., Lorenzini, E. C., Lopez-Rebollal, O., and Ruiz, M., “A New Kind of Dynamic Instability in Electrodynamic Tethers,” *Journal of the Astronautical Sciences*, Vol. 48, No. 4, 2000, pp. 449-476.
- Prag, A. B., “A Comparison of the MSIS and Jacchia-70 Models with Measured Atmospheric Density Data in the 120 to 200 km Altitude Range,” Aerospace Corp., El Segundo, CA, 1983
- Gong, Q., Fahroo, F., Ross, I.M., “Spectral Algorithm for Pseudospectral Methods in Optimal Control,” *Journal of Guidance, Control, and Dynamics*, Vol. 31, No. 3, 2008.
- Stevens, R. S., “Optimal Control of Electrodynamic Tether Satellites” Air Force Institute of Technology, Wright-Patterson AFB, Ohio, June 2008
- Tragesser, S. G., and San, H., “Orbital Maneuvering with Electrodynamic Tethers,” *Journal of Guidance, Control, and Dynamics*, Vol. 26, No. 5, 2003, pp. 805-810.
- Trefethen, L. N., *Spectral Methods in Matlab*, SIAM, Philadelphia, PA, 2000
- Vallado, D., A., “Fundamentals of Astrodynamics and Applications”, 3rd Ed., Microcosm Press, Hawthorne, CA, 2007.
- Williams, P., “Optimal Orbital Transfer with Electrodynamic Tether,” *Journal of Guidance, Control, and Dynamics*, Vol. 28, No. 2, 2005, pp. 369-371.
- Vallado, D., A., “Fundamentals of Astrodynamics and Applications”, 3rd Ed., Microcosm Press, Hawthorne, CA, 2007.
- “Space Math @ NASA” <http://spacemath.gsfc.nasa.gov/weekly/5Page35.pdf>
- “Orbital Debris Quarterly News” Volume 15 Issue 1, January 2011, NASA JSC
- “Dealing with Galaxy 15: Zombiesats and on-orbit servicing” – Brian Weeden, The Space Review, 24 May, 2010, <http://goes.gsfc.nasa.gov/text/Zombiesats.pdf>
- “Space Transportation Costs: Trends in Price Per Pound to Orbit 1990-2000”, Futron Corporation, September 6, 2002.

## Glossary

$a$	=	Semi-major axis
$\mathbf{A}_1$	=	Environmental response vector – instantaneous dynamics
$\mathbf{B}_1$	=	Control response vector – instantaneous dynamics
$\mathbf{A}_2$	=	Environmental response vector – averaged dynamics
$\mathbf{B}_2$	=	Control response vector – averaged dynamics
$\mathbf{A}_3$	=	Environmental response vector – linearized dynamics
$\mathbf{B}_3$	=	Control response vector – linearized dynamics
$\mathbf{B}$	=	Local magnetic field vector
$B^*$	=	Inverse ballistic coefficient
$e$	=	Eccentricity
$\mathbf{F}_e$	=	Resultant electromagnetic force vector
$\mathbf{F}$	=	Force vector in RSW frame
$f$	=	Accelerations in RSW frame
$h$	=	First equinoctial element
$i$	=	Inclination
$I$	=	Time variant control current
$k$	=	Second equinoctial element
$\mathbf{L}$	=	Tether length vector
$\mu_0$	=	magnetic constant
$\mu$	=	Standard gravitational parameter
$n$	=	Mean motion
$\omega$	=	Argument of perigee
$\Omega$	=	Right ascension of ascending node
$p$	=	Semi-parameter
$\mathbf{Q}$	=	State weighting matrix
$\mathbf{R}$	=	Control weighting matrix
$t$	=	Short scale time
$T$	=	Long scale time
$v$	=	True anomaly
$\mathbf{u}$	=	Control coefficient vector
$\Psi$	=	Control periodic function vector

## Appendix A

### DERIVATION OF EQUATIONS OF MOTION

All equations references are from “Fundamentals of Astrodynamics and Applications” by David

A. Vallado. We begin with the Gaussian VOP equations from Vallado.

$$\begin{aligned}\frac{da}{dt} &= \frac{2}{n\sqrt{1-e^2}} \left[ e \sin(\nu) f_R + \frac{p}{r} f_S \right] \\ \frac{de}{dt} &= \frac{\sqrt{1-e^2}}{na} \left[ \sin(\nu) f_R + \left( \cos(\nu) + \frac{e + \cos(\nu)}{1 + e \cos(\nu)} \right) f_S \right] \\ \frac{di}{dt} &= \frac{r \cos(\nu + \omega)}{na^2 \sqrt{1-e^2}} f_W \\ \frac{d\Omega}{dt} &= \frac{r \sin(\nu + \omega)}{na^2 \sqrt{1-e^2} \sin(i)} f_W \\ \frac{d\omega}{dt} &= \frac{\sqrt{1-e^2}}{nae} \left[ -\cos(\nu) f_R + \sin(\nu) \left( 1 + \frac{r}{p} \right) f_S \right] - \frac{r \cot(i) \sin(\nu + \omega)}{h} f_W \\ \frac{d\nu}{dt} &= \frac{na^2}{r^3} \sqrt{1-e^2} + \frac{\sqrt{1-e^2}}{nae} \cos(\nu) f_R - \frac{\sqrt{1-e^2}}{nae} \frac{2 + e \cos(\nu)}{1 + e \cos(\nu)} f_S\end{aligned}$$

We now undergo a process of applying several transformations. These are:

- Replacement of  $e, \omega$  with  $h, k$  (partial equinoctial set).
  - $\dot{h} = \dot{e} \sin(\omega) + e \cos(\omega)$
  - $\dot{k} = \dot{e} \cos(\omega) - e \sin(\omega)$
- Nearly circular orbits ( $e \ll 1$ ).
  - This allows us to simplify many expressions containing  $\mathcal{O}(e^2)$  terms. Also terms dividing by  $(1 - e)$  become multiplied by  $(1 + e)$  etc...
- Replacement of time as independent variable.
  - Multiply each equation of the system dynamics by  $\frac{dt}{d\nu} = \sqrt{\frac{a^3}{\mu}} (1 - 2e \cos \nu)$

This leads us to the reduced dynamics in the partial equinoctial set.

$$\begin{aligned}
\frac{da}{dv} &= \frac{2a^3}{\mu_{\oplus}} \left[ e \sin(\nu) f_R + (1 - e \cos(\nu)) f_S \right] \\
\frac{di}{dv} &= \frac{a^2}{\mu_{\oplus}} (1 - 3e \cos(\nu)) \cos(\nu + \omega) f_W \\
\frac{d\Omega}{dv} &= \frac{a^2}{\mu_{\oplus}} (1 - 3e \cos(\nu)) \frac{\sin(\nu + \omega)}{\sin(i)} f_W \\
\frac{dh}{dv} &= \frac{a^2}{\mu_{\oplus}} \begin{bmatrix} -\cos(\nu + \omega) - h \sin(2\nu) - 2k \cos^2(\nu) \\ 2 \sin(\nu + \omega) + h \sin^2(\nu) - 5k \sin(\nu) \cos(\nu) - 4h \cos^2(\nu) \\ -k \sin(\nu + \omega) \cot(i) \end{bmatrix}^T \begin{bmatrix} f_R \\ f_S \\ f_W \end{bmatrix} \\
\frac{dk}{dv} &= \frac{a^2}{\mu_{\oplus}} \begin{bmatrix} \sin(\nu + \omega) - k \sin(2\nu) - 2h \cos^2(\nu) \\ 2 \cos(\nu + \omega) + k \sin^2(\nu) + 5h \sin(\nu) \cos(\nu) - 4k \cos^2(\nu) \\ h \sin(\nu + \omega) \cot(i) \end{bmatrix}^T \begin{bmatrix} f_R \\ f_S \\ f_W \end{bmatrix}
\end{aligned}$$

The accelerations due to electrodynamic interactions are a result of the Lorentz force,  $\mathbf{F} = I\mathbf{L} \times \mathbf{B}$  where  $\mathbf{L}$  is of magnitude  $L$  in the Radial direction and  $\mathbf{B}$  is the local geomagnetic field

vector. We used a non-tilted dipole model,  $\mathbf{B} = \frac{\gamma_m \mu_0}{r^3} \begin{bmatrix} -2 \sin(\nu + \omega) \sin(i) \\ \cos(\nu + \omega) \sin(i) \\ \cos(i) \end{bmatrix}$  ( $\text{N} \cdot \text{A}^{-1} \text{m}^{-1}$ ), though any

model could be used. We need accelerations rather than forces, so we write  $f = \mathbf{F}/m$  to express the accelerations in the LVLH frame.

$$f_{\text{ether}} = \frac{IL\gamma_m\mu_0}{ma^3} (1 + 3e \cos(\nu)) \begin{bmatrix} 0 \\ -\cos(i) \\ \cos(\nu + \omega) \sin(i) \end{bmatrix} \quad (\text{m} \cdot \text{s}^{-2})$$

To characterize the accelerations due to drag we first express the force as

$\mathbf{F}_{\text{drag}} = -\frac{1}{2} C_D A \rho V^2 \hat{\mathbf{V}}$ . We can determine the velocity at any point via

$$V = \sqrt{\frac{2\mu}{r} - \frac{\mu}{a}}$$

The direction of the velocity vector is defined by the flight path angle,  $\phi_{fpa}$ . This is the angle measured from the local horizontal to the velocity vector.

$$\hat{\mathbf{V}} = \begin{bmatrix} \sin(\phi_{fpa}) \\ \cos(\phi_{fpa}) \\ 0 \end{bmatrix} \quad (4.2)$$

It is thus unnecessary to define  $\phi_{fpa}$  exactly as it is much easier to define the sine and cosine of this angle. From Vallado we can say:

$$\sin(\phi_{fpa}) = \frac{e \sin(\nu)}{\sqrt{1 + 2e \cos(\nu) + e^2}} \quad (4.3)$$

$$\cos(\phi_{fpa}) = \frac{1 + e \cos(\nu)}{\sqrt{1 + 2e \cos(\nu) + e^2}} \quad (4.4)$$

From this we can fully express the drag acceleration. Before we do this, we introduce a new variable,  $B^*$ . We define this “inverse ballistic coefficient” as  $B^* = \frac{C_D A}{m}$ . Finally we express the

drag accelerations as

$$f_D = -\frac{1}{2} B^* \rho \frac{\mu}{a} \begin{bmatrix} e \sin(\nu) \\ 1 + 2e \cos(\nu) \\ 0 \end{bmatrix} \quad (4.5)$$

Putting together the tether and drag forces with the general system dynamics we arrive at the following equations,

$$\begin{aligned} \frac{da}{dv} &= 2C_m \cos(i)(1 + 2e \cos(\nu)) \cdot I - B^* \rho a^2 (1 + e \cos(\nu)) \\ \frac{di}{dv} &= \frac{-C_m}{a} \sin(i) \cos^2(\nu + \omega) \cdot I \\ \frac{d\Omega}{dv} &= \frac{-C_m}{a} \sin(\nu + \omega) \cos(\nu + \omega) \cdot I \\ \frac{dh}{dv} &= \frac{C_m}{a} \cos(i) \left[ \frac{3h}{2} + \frac{2h}{e} \cos(\nu) + \frac{2k}{e} \sin(\nu) + \left( \frac{h}{2} + \frac{hk^2}{e^2} \right) \cos(2\nu) + \left( \frac{k}{2} + \frac{k(k^2 - h^2)}{2e^2} \right) \sin(2\nu) \right] \cdot I \\ &\quad - \frac{1}{2} B^* \rho a \left( h + \frac{2h}{e} \cos(\nu) + \frac{2k}{e} \sin(\nu) - h \cos(2\nu) - k \sin(2\nu) \right) \\ \frac{dk}{dv} &= \frac{C_m}{a} \cos(i) \left[ \frac{3k}{2} + \frac{2k}{e} \cos(\nu) - \frac{2h}{e} \sin(\nu) + \left( \frac{k}{2} - \frac{kh^2}{e^2} \right) \cos(2\nu) - \left( \frac{h}{2} + \frac{h(k^2 - h^2)}{2e^2} \right) \sin(2\nu) \right] \cdot I \\ &\quad - \frac{1}{2} B^* \rho a \left( k + \frac{2k}{e} \cos(\nu) - \frac{2h}{e} \sin(\nu) - k \cos(2\nu) + h \sin(2\nu) \right) \end{aligned}$$

Where  $C_m = \frac{L\gamma_m\mu_0}{m\mu_\oplus}$ . This is a very cumbersome set of equations to work with. We can notice

many common terms, notably, sine and cosine of  $v$  or  $2v$ . If we extract these terms and write these five equations as matrices, we arrive at the following,

$$\frac{d\mathbf{x}}{dv} = C_m \begin{matrix} \text{x} \\ \begin{bmatrix} 2\cos(i) & 4e\cos(i) & 0 & 0 & 0 \\ -\frac{1}{2a}\sin(i) & 0 & 0 & -\frac{k^2-h^2}{2ae^2}\sin(i) & \frac{hk}{ae^2}\sin(i) \\ 0 & 0 & 0 & -\frac{hk}{ae^2} & -\frac{k^2-h^2}{2ae^2} \\ \frac{3h}{2a}\cos(i) & \frac{2h}{ae}\cos(i) & \frac{2k}{ae}\cos(i) & \left(\frac{h}{2a} + \frac{hk^2}{ae^2}\right)\cos(i) & \left(\frac{k}{2a} + \frac{k(k^2-h^2)}{2ae^2}\right)\cos(i) \\ \frac{3k}{2a}\cos(i) & \frac{2k}{ae}\cos(i) & -\frac{2h}{ae}\cos(i) & \left(\frac{k}{2a} - \frac{kh^2}{ae^2}\right)\cos(i) & -\left(\frac{h}{2a} + \frac{h(k^2-h^2)}{2ae^2}\right)\cos(i) \end{bmatrix} \begin{bmatrix} 1 \\ \cos(v) \\ \sin(v) \\ \cos(2v) \\ \sin(2v) \end{bmatrix} I \end{matrix}$$

$$-B^* \rho a \begin{bmatrix} a & ae & 0 & 0 & 0 \\ 0 & 0 & 0 & 0 & 0 \\ 0 & 0 & 0 & 0 & 0 \\ \frac{h}{2} & \frac{h}{e} & \frac{k}{e} & -h & -k \\ \frac{k}{2} & \frac{k}{e} & -\frac{h}{e} & -k & h \end{bmatrix} \begin{bmatrix} 1 \\ \cos(v) \\ \sin(v) \\ \cos(2v) \\ \sin(2v) \end{bmatrix}$$

Which we can reduce compactly to the following matrix form which is the basis of the remaining analysis,

$$\frac{d\mathbf{x}}{dv} = \mathbf{A}_1(\mathbf{x}, v) + \mathbf{B}_1(\mathbf{x}, v)I$$

## Appendix B

### METHOD OF AVERAGING – MATRICES

The purpose of this appendix is to define the matrices found when applying the method of averaging. Those matrices would be  $\mathbf{A}$  and  $\mathbf{B}$  and their many variations, and the  $\Psi\text{-}\Phi$  product.

$$\Psi^T = \text{sgn}([1 \quad \cos(\nu) \quad \sin(\nu) \quad \cos(2\nu) \quad \sin(2\nu)])$$

$$\Phi^T = [1 \quad \cos(\nu) \quad \sin(\nu) \quad \cos(2\nu) \quad \sin(2\nu)]$$

$$\mathbf{A}_1(\mathbf{x}) = -B^* \rho a \begin{bmatrix} a & ae & 0 & 0 & 0 \\ 0 & 0 & 0 & 0 & 0 \\ 0 & 0 & 0 & 0 & 0 \\ \frac{h}{2} & \frac{h}{e} & \frac{k}{e} & -h & -k \\ \frac{k}{2} & \frac{k}{e} & -\frac{h}{e} & -k & h \end{bmatrix}$$

$$\mathbf{A}_1(\mathbf{x}, \nu) = \mathbf{A}_1'(\mathbf{x})\Phi(\nu)$$

$$\mathbf{B}_1'(\mathbf{x}) = C \begin{bmatrix} 2\cos(i) & 4e\cos(i) & 0 & 0 & 0 \\ -\frac{1}{2a}\sin(i) & 0 & 0 & -\frac{k^2-h^2}{2ae^2}\sin(i) & \frac{hk}{ae^2}\sin(i) \\ 0 & 0 & 0 & -\frac{hk}{ae^2} & -\frac{k^2-h^2}{2ae^2} \\ \frac{3h}{2a}\cos(i) & \frac{2h}{ae}\cos(i) & \frac{2k}{ae}\cos(i) & \left(\frac{h}{2a} + \frac{hk^2}{ae^2}\right)\cos(i) & \left(\frac{k}{2a} + \frac{k(k^2-h^2)}{2ae^2}\right)\cos(i) \\ \frac{3k}{2a}\cos(i) & \frac{2k}{ae}\cos(i) & -\frac{2h}{ae}\cos(i) & \left(\frac{k}{2a} - \frac{kh^2}{ae^2}\right)\cos(i) & -\left(\frac{h}{2a} + \frac{h(k^2-h^2)}{2ae^2}\right)\cos(i) \end{bmatrix}$$

$$\mathbf{B}_1(\mathbf{x}, \nu) = \mathbf{B}_1'(\mathbf{x})\Phi(\nu)\Psi^T(\nu)$$

Now we apply the method of averaging, whereby the  $\mathbf{A}'$  and  $\mathbf{B}'$  matrices are not dependent on time, and thus can be pulled out of the integral. This leaves us to integrate  $\Phi$ , and  $\Phi\Psi^T$ .

And those integrals are:

$$\frac{1}{2\pi N} \int_0^{2\pi N} \Phi d\nu = \begin{bmatrix} 1 \\ 0 \\ 0 \\ 0 \\ 0 \end{bmatrix}$$

$$\frac{1}{2\pi N} \int_0^{2\pi N} \Phi(\nu) \Psi^T(\nu) d\nu$$

$$\frac{1}{2\pi N} \int_0^{2\pi N} \begin{bmatrix} 1 & \operatorname{sgn}(\cos(\nu)) & \operatorname{sgn}(\sin(\nu)) & \operatorname{sgn}(\cos(2\nu)) & \operatorname{sgn}(\sin(2\nu)) \\ \cos(\nu) & |\cos(\nu)| & \operatorname{sgn}(\sin(\nu))\cos(\nu) & \operatorname{sgn}(\cos(2\nu))\cos(\nu) & \operatorname{sgn}(\sin(2\nu))\cos(\nu) \\ \sin(\nu) & \operatorname{sgn}(\cos(\nu))\sin(\nu) & |\sin(\nu)| & \operatorname{sgn}(\cos(2\nu))\sin(\nu) & \operatorname{sgn}(\sin(2\nu))\sin(\nu) \\ \cos(2\nu) & \operatorname{sgn}(\cos(\nu))\cos(2\nu) & \operatorname{sgn}(\sin(\nu))\cos(2\nu) & |\cos(2\nu)| & \operatorname{sgn}(\sin(2\nu))\cos(2\nu) \\ \sin(2\nu) & \operatorname{sgn}(\cos(\nu))\sin(2\nu) & \operatorname{sgn}(\sin(\nu))\sin(2\nu) & \operatorname{sgn}(\cos(2\nu))\sin(2\nu) & |\sin(2\nu)| \end{bmatrix} d\nu$$

$$\frac{1}{2\pi N} \int_0^{2\pi N} \Phi(\nu) \Psi^T(\nu) d\nu = \begin{bmatrix} 1 & 0 & 0 & 0 & 0 \\ 0 & 2/\pi & 0 & 0 & 0 \\ 0 & 0 & 2/\pi & 0 & 0 \\ 0 & 0 & 0 & 2/\pi & 0 \\ 0 & 0 & 0 & 0 & 2/\pi \end{bmatrix}$$

That lets us define  $\mathbf{A}_2$  and  $\mathbf{B}_2$  as the following:

$$\mathbf{A}_2 = \frac{1}{2\pi N} \mathbf{A}'_1 \int_0^{2\pi N} \Phi(\nu) d\nu \quad \text{and} \quad \mathbf{B}_2 = \frac{1}{2\pi N} \mathbf{B}'_1 \int_0^{2\pi N} \Phi(\nu) \Psi^T(\nu) d\nu \cdot \mathbf{u}$$

$$\mathbf{A}_2(\mathbf{x}) = -B^* \rho a \begin{bmatrix} a \\ 0 \\ 0 \\ \frac{1}{2}h \\ \frac{1}{2}k \end{bmatrix}$$

$$\mathbf{B}_2(\mathbf{x}) = \frac{C_m}{\pi a} \begin{bmatrix} 2\pi a \cos(i) & 8ae \cos(i) & 0 & 0 & 0 \\ -\frac{1}{2}\pi \sin(i) & 0 & 0 & -\frac{k^2 - h^2}{e^2} \sin(i) & \frac{2hk}{e^2} \sin(i) \\ 0 & 0 & 0 & -\frac{2hk}{e^2} & -\frac{k^2 - h^2}{e^2} \\ \frac{3\pi h}{2} \cos(i) & \frac{4h}{e} \cos(i) & \frac{4k}{e} \cos(i) & \left(\frac{h}{1} + \frac{2hk^2}{e^2}\right) \cos(i) & \left(\frac{k}{1} + \frac{k(k^2 - h^2)}{e^2}\right) \cos(i) \\ \frac{3\pi k}{2} \cos(i) & \frac{4k}{e} \cos(i) & -\frac{4h}{e} \cos(i) & \left(\frac{k}{1} - \frac{2kh^2}{e^2}\right) \cos(i) & -\left(\frac{h}{1} + \frac{h(k^2 - h^2)}{e^2}\right) \cos(i) \end{bmatrix}$$

# Appendix C

## LINEARIZATION

Beginning with the averaged equations of motion

$$\frac{d\mathbf{x}}{dT} = \mathbf{A}_2(\mathbf{x}) + \mathbf{B}_2(\mathbf{x})\mathbf{u}$$

we apply a first order approximation for  $\mathbf{f}(\mathbf{x} + \delta\mathbf{x}, \mathbf{u} + \delta\mathbf{u})$  as the following:

$$\mathbf{f}(\mathbf{x} + \delta\mathbf{x}, \mathbf{u} + \delta\mathbf{u}) = \mathbf{f}(\mathbf{x}, \mathbf{u}) + \mathbf{f}_x \delta\mathbf{x} + \mathbf{f}_u \delta\mathbf{u}$$

$\mathbf{f}_x$  and  $\mathbf{f}_u$  are the Jacobian of  $d\mathbf{x}/dT$  with respect to the state vector,  $\mathbf{x}$ , and the control vector,  $\mathbf{u}$ .

The second term is simple enough to compute by hand because it reduces to  $\mathbf{B}_3 = \frac{d(\mathbf{A}_2 + \mathbf{B}_2\mathbf{u})}{d\mathbf{u}} = \mathbf{B}_2$  because neither  $\mathbf{A}_2$  nor  $\mathbf{B}_2$  are functions of  $\mathbf{u}$ .

The first term however, is significantly more difficult. Both  $\mathbf{A}_2$  and  $\mathbf{B}_2$  are functions of the state vector and thus have filled Jacobians. This operation was done with the help of a symbolic manipulator to ensure no human errors were introduced in the transcription of the equations due to their complexity. Also, even in simplified expressions, these matrices are too large to display properly on a page and for that reason will not shown in “equation form”. The best definition of  $\mathbf{A}_3$  is as  $\mathbf{A}_3 = \frac{d(\mathbf{A}_2 + \mathbf{B}_2\mathbf{u})}{d\mathbf{x}} = \mathbf{f}_x$ . The matrix is

presented element-wise in the form used in the computer code.

### First Row, Columns 1-5

```
-2*Bs*p*a,  
-2*Cm*sin(i)*u1-8*Cm/pi*(h2+k2)(1/2)*sin(i)*u2,  
0,  
8*Cm/pi/(h2+k2)(1/2)*cos(i)*u2*h,  
8*Cm/pi/(h2+k2)(1/2)*cos(i)*u2*k;
```

### Second Row, Columns 1-5

```
½*Cm/a2*sin(i)*u1-Cm/pi/a2*(-k2+h2)/(h2+k2)*sin(i)*u4-2*Cm/pi/a2*h*k/(h2+k2)*sin(i)*u5,  
-1/2*Cm/a*cos(i)*u1+Cm/pi/a*(-k2+h2)/(h2+k2)*cos(i)*u4+2*Cm/pi/a*h*k/(h2+k2)*cos(i)*u5,  
0,
```

$$2^*Cm/pi/a*h/(h^2+k^2)*sin(i)*u4-2^*Cm/pi/a*(-k^2+h^2)/(h^2+k^2)^2*sin(i)*u4+2^*Cm/pi/a*k/(h^2+k^2)*sin(i)*u5-4^*Cm/pi/a*h^2*k/(h^2+k^2)^2*sin(i)*u5,$$

$$-2^*Cm/pi/a*k/(h^2+k^2)*sin(i)*u4-2^*Cm/pi/a*(-k^2+h^2)/(h^2+k^2)^2*sin(i)*u4+2^*Cm/pi/a*h/(h^2+k^2)*sin(i)*u5-4^*Cm/pi/a*h*k^2/(h^2+k^2)^2*sin(i)*u5;$$

### Third Row, Columns 1-5

$$2^*Cm/pi/a^2*h*k/(h^2+k^2)*u4-Cm/pi/a^2*(-k^2+h^2)/(h^2+k^2)*u5,$$

0,

0,

$$-2^*Cm/pi/a*k/(h^2+k^2)*u4+4^*Cm/pi/a*h^2*k/(h^2+k^2)^2*u4+2^*Cm/pi/a*h/(h^2+k^2)*u5-2^*Cm/pi/a*(-k^2+h^2)/(h^2+k^2)^2*u5*h,$$

$$-2^*Cm/pi/a*h/(h^2+k^2)*u4+4^*Cm/pi/a*h*k^2/(h^2+k^2)^2*u4-2^*Cm/pi/a*k/(h^2+k^2)*u5-2^*Cm/pi/a*(-k^2+h^2)/(h^2+k^2)^2*u5*k;$$

### Fourth Row, Columns 1-5

$$-1/2^*Bs*p*h-3/2^*Cm/a^2*h*cos(i)*u1-4^*Cm/pi/a^2*h/(h^2+k^2)^(1/2)*cos(i)*u2-4^*Cm/pi/a^2*k/(h^2+k^2)^(1/2)*cos(i)*u3-Cm/pi/a^2*(h+2*h*k^2/(h^2+k^2))*cos(i)*u4-Cm/pi/a^2*(k+k*(k^2-h^2)/(h^2+k^2))*cos(i)*u5,$$

$$-3/2^*Cm/a*h*sin(i)*u1-4^*Cm/pi/a*h/(h^2+k^2)^(1/2)*sin(i)*u2-4^*Cm/pi/a*k/(h^2+k^2)^(1/2)*sin(i)*u3-Cm/pi/a*(h+2*h*k^2/(h^2+k^2))*sin(i)*u4-Cm/pi/a*(k+k*(k^2-h^2)/(h^2+k^2))*sin(i)*u5,$$

0,

$$-1/2^*Bs*p*a+3/2^*Cm/a*cos(i)*u1+4^*Cm/pi/a/(h^2+k^2)^(1/2)*cos(i)*u2-4^*Cm/pi/a*h^2/(h^2+k^2)^(3/2)*cos(i)*u2-4^*Cm/pi/a*k/(h^2+k^2)^(3/2)*cos(i)*u3+h*Cm/pi/a*(1+2*k^2/(h^2+k^2))-4^*h^2*k^2/(h^2+k^2)^2*cos(i)*u4+Cm/pi/a*(-2*k*h/(h^2+k^2)-2*k*(k^2-h^2)/(h^2+k^2)^2*h)*cos(i)*u5,$$

$$-4^*Cm/pi/a*h/(h^2+k^2)^(3/2)*cos(i)*u2*k+4^*Cm/pi/a/(h^2+k^2)^(1/2)*cos(i)*u3-4^*Cm/pi/a*k^2/(h^2+k^2)^(3/2)*cos(i)*u3+Cm/pi/a*(4*k*h/(h^2+k^2))-4^*h*k^3/(h^2+k^2)^2*cos(i)*u4+Cm/pi/a*(1+(k^2-h^2)/(h^2+k^2)+2*k^2/(h^2+k^2)-2*k^2*(k^2-h^2)/(h^2+k^2)^2)*cos(i)*u5;...$$

### Fifth Row, Columns 1-5

$$-1/2^*Bs*p*k-3/2^*Cm/a^2*k*cos(i)*u1-4^*Cm/pi/a^2*k/(h^2+k^2)^(1/2)*cos(i)*u2+4^*Cm/pi/a^2*h/(h^2+k^2)^(1/2)*cos(i)*u3-Cm/pi/a^2*(k-2*k*h^2/(h^2+k^2))*cos(i)*u4-Cm/pi/a^2*(-h-h*(k^2-h^2)/(h^2+k^2))*cos(i)*u5,$$

$$-3/2^*Cm/a*k*sin(i)*u1-4^*Cm/pi/a*k/(h^2+k^2)^(1/2)*sin(i)*u2+4^*Cm/pi/a*h/(h^2+k^2)^(1/2)*sin(i)*u3-Cm/pi/a*(k-2*k*h^2/(h^2+k^2))*sin(i)*u4-Cm/pi/a*(-h-h*(k^2-h^2)/(h^2+k^2))*sin(i)*u5,$$

0,

$$-4^*Cm/pi/a*h/(h^2+k^2)^(3/2)*cos(i)*u2*k-4^*Cm/pi/a/(h^2+k^2)^(1/2)*cos(i)*u3+4^*Cm/pi/a*h^2/(h^2+k^2)^(3/2)*cos(i)*u3+Cm/pi/a*(-4*k*h/(h^2+k^2)+4*k*h^3/(h^2+k^2)^2)*cos(i)*u4+Cm/pi/a*(-1-(k^2-h^2)/(h^2+k^2)+2*h^2/(h^2+k^2)+2*h^2*(k^2-h^2)/(h^2+k^2)^2)*cos(i)*u5,$$

$$-1/2^*Bs*p*a+3/2^*Cm/a*cos(i)*u1+4^*Cm/pi/a/(h^2+k^2)^(1/2)*cos(i)*u2-4^*Cm/pi/a*k^2/(h^2+k^2)^(3/2)*cos(i)*u2+4^*Cm/pi/a*k/(h^2+k^2)^(3/2)*cos(i)*u3+h*Cm/pi/a*(1-2*h^2/(h^2+k^2)+4*h^2*k^2/(h^2+k^2)^2)*cos(i)*u4+Cm/pi/a*(-2*k*h/(h^2+k^2)+2*k*(k^2-h^2)/(h^2+k^2)^2*h)*cos(i)*u5];$$